Materials Horizons

ROYAL SOCIETY OF CHEMISTRY

COMMUNICATION

View Article Online
View Journal | View Issue

Cite this: *Mater. Horiz.*, 2025, 12, 4229

Received 19th December 2024,
Accepted 18th March 2025

DOI: 10.1039/d4mh01862a

rsc.li/materials-horizons

Puncture-resistant hydrogels with high mechanical performance achieved by the supersaturated salt†

Bo Tang,[ab] Jian Hu,[ab] Zijian Zhao,[ab] Shuo Li,[ab] Hongying Lv *[a] and Xiaoniu Yang[ab]

Sufficient mechanical performance is the basic requirement for load-bearing and damage-resistant materials. However, the simultaneous optimization of mechanical properties is usually difficult in a single hydrogel. Herein, a supersaturated salt was employed to enhance the mechanical performance and damage resistance of hydrogels. By immersing the pre-formed hydrogel based on hydrophobic associations into supersaturated Na_2SO_4 solution (3.3 M), high-density and strong hydrophobic associations were constructed simultaneously in the network due to the contraction of hydrophilic chains and improvement of hydrophobic associations. Compared to the pristine hydrogel, this salt-treated hydrogel was transparent and showed a simultaneous enhancement in stiffness (E of 253 ± 7 MPa), strength (σ of 12.65 ± 0.07 MPa), and toughness (Γ of 19.6 ± 3.2 MJ m^{-3}). It also displayed remarkable puncture and tear resistance with a puncture force of 66 N, a puncture energy of 370 mJ, and a tearing energy of 34 kJ m^{-2}. This work provides a simple method to simultaneously optimize the contradictory mechanical properties and puncture resistance in a single hydrogel.

New concepts

In this manuscript, we propose for the first time, a method of supersaturated salt soaking to improve the puncture resistance and mechanical performance of hydrogels. Soaking in supersaturated sodium sulfate solution simultaneously increases the strength and density of hydrophobic associations, leading to the high density and appropriate strength of hydrophobic associations in the network. Therefore, the salt-treated hydrogels are transparent and show a simultaneous enhancement in stiffness, strength, and toughness. More importantly, this network structure endows the hydrogel with excellent puncture resistance. Its maximum puncture force value is 66 N, and the puncture energy is 370 mJ. This study may provide a simple method of optimizing the mechanical performance and puncture resistance of hydrophobic aggregation-based hydrogels for load-bearing and puncture-resistant materials.

1. Introduction

Hydrogels consisting of polymer networks and water have attracted increasing attention due to their unique structure.[1–3] However, the conventional hydrogels often face mechanical damage (such as tears or punctures from sharp objects) due to their weak network. High mechanical performance is essential for hydrogels to resist mechanical damage: on one hand, the high strength and stiffness can effectively prevent sharp object from penetrating hydrogels; on the other hand, the high toughness enables hydrogels to absorb more energy to inhibit damage propagation.[4] Nevertheless, the toughness, stiffness, and strength have different requirements for the crosslinks,[1,2,5] where high toughness needs dynamic sacrificial crosslinks (hydrogen bonding,[6,7] electrostatic interactions,[8,9] and hydrophobic interactions[10–13]), to dissipate energy by destroying themselves under load, while high stiffness and strength demand dense strong crosslinks (chemical bonds) to resist deformation and withstand load.[14,15] A promising strategy for improving them simultaneously is to build high-density and strong dynamic crosslinks in the homogenous network.[16] The highly crosslinked network could restrain the polymer chains among strong dynamic crosslinks at the initial deformation to enhance the stiffness, and the destruction of substantial dynamic crosslinks could bear load and dissipate energy at large deformation to improve strength and toughness.[17,18] However, the common dynamic bonds are often too weak to resist deformation, and it is necessary to develop strong dynamic crosslinks in the highly crosslinked network.

Hydrophobic association is one of the most widely explored dynamic physical interactions because of its adjustable strength, multi-functionality, and deformation under load.[11,19,20] Many strong and tough hydrogels have been prepared *via* the free radical copolymerization of hydrophobic and hydrophilic

[a] State Key Laboratory of Polymer Science and Technology, Changchun Institute of Applied Chemistry, Chinese Academy of Sciences, Changchun, 130022, P. R. China. E-mail: hongyinglv@ciac.ac.cn
[b] School of Applied Chemistry and Engineering, University of Science and Technology of China, Jinzhai Road No 96, Hefei, 230026, P. R. China

† Electronic supplementary information (ESI) available. See DOI: https://doi.org/10.1039/d4mh01862a

monomers and the following solvent exchange method.[10,21–23] These hydrophobic associations are spontaneously formed during solvent exchange process *via* the self-aggregation of hydrophobic moieties of copolymers.[10,11,19–24] Their distribution, density, and strength that greatly affect the mechanical performance highly depend on the copolymer structure, which is mainly determined by the structure and mole ratio of comonomers in the polymerization system.[19–23,25] However, the copolymer structure has an opposite effect on the strength and density of hydrophobic associations: increasing the hydrophobicity of copolymer often leads to strong but fewer hydrophobic associations, while decreasing the hydrophobicity induces weak but more hydrophobic associations. Thus, constructing high-density and suitably strong hydrophobic association in a network is still a challenge.

In this work, we proposed a method to simultaneously increase the density and strength of hydrophobic associations by utilizing the supersaturated salt. A series of hydrogels based on highly dense and suitably strong hydrophobic associations were formed by copolymerizing hydrophobic 2-aminoethyl methacrylate isopropyl carbamate (IMA) and hydrophilic acrylamide (AAm) followed by a soaking process in Na_2SO_4 solution. The space between hydrophobic aggregates and their strength in hydrogels in a fixed monomer ratio could be simply adjusted by the concentration of Na_2SO_4 solution due to the Hofmeister effect, which causes the chain contraction between hydrophobic aggregates and their self-strengthening simultaneously. The hydrogel crosslinked by highly dense and strong hydrophobic associations was stiff, strong, and tough with a modulus of 253 MPa, a fracture strength of 12.65 MPa, a toughness of 19.6 MJ m^{-3}. It also exhibited good tear and puncture resistance with a maximum tear energy of 34 kJ m^{-2}, a puncture force of 66 N and a maximum puncture energy of 370 mJ. This study may provide a simple method of optimizing the mechanical performance and damage resistance of hydrophobic aggregation-based hydrogels for load-bearing and puncture-resistant materials.

2. Experimental section

2.1 Materials

2-Isocyanomethacrylate (98%), 2-propanol, dibutyltin dilaurate (DBTD), *N*,*N*′-methylenebisacrylamide (MBAA) (98%), acrylamide (AAm), 2,2′-azobis(2-methylpropanenitrile) (AIBN) (98%), dimethyl sulfoxide (DMSO), butyl acrylate (BA), 2-ethylhexyl acrylate (2EA), and anhydrous sodium sulfate (Na_2SO_4) were purchased from Energy Chemical Company and used as received. Dichloromethane (DCM) was distilled from CaH_2 before use.

2.2 Synthesis of P(IMA-*co*-AAm)–Na_2SO_4 hydrogels

The monomer IMA, and the P(IMA-*co*-AAm), P(BA-*co*-AAm), and P(2EA-*co*-AAm) hydrogels were synthesized according to our previously described method.[11] For example, the P(IMA$_1$-*co*-AAm$_{1.5}$) hydrogel was prepared as follows: IMA (3.50 g, 16.15 mmol), AAm (1.75 g, 24.23 mmol), MBAA (126 mg, 0.80 mmol), and AIBN (20 mg, 0.12 mmol) were dissolved in DMSO/H_2O (26.4 mL, 10/1, v/v). The solution was deoxygenated in liquid nitrogen under vacuum and then injected into a rectangular glass mold for polymerizing at 60 °C for 10 hours. After polymerization, the obtained gel was cut into a dumbbell shape using a cutter and immersed in water until reaching equilibrium to get the hydrogel. The water was replaced four times on the first day and twice per day for 3 days during immersion. Finally, the P(IMA$_1$-*co*-AAm$_{1.5}$)–Na_2SO_4 hydrogels were gained by immersing the as-prepared hydrogels in the Na_2SO_4 solutions with different concentrations (0 M, 0.5 M, 1 M, 1.5 M, 2 M, 2.5 M, and 3.3 M) for 48 h. The supersaturated Na_2SO_4 solution (>2.3 M) was prepared by heating the solution at 60 °C for 3 h and then cooling down to room temperature. The PAAm hydrogel was prepared according to the previous literature,[26] and then underwent the above salt solution treatment.

2.3 Characterization

The ^{1}H NMR spectra were recorded using a Bruker AV400 NMR. Deuterated DMSO (DMSO-d_6) was used as the solvent. The attenuated total reflection Fourier transform infrared (ATR-FTIR) spectra were obtained using a FTIR spectrophotometer (Bruker INVENIO R) with ATR attachments (equipped with a diamond crystal). The hydrogels were lyophilized before testing in a range of 4000–400 cm^{-1} with a resolution of 4 cm^{-1} and 128 scans. The relative swelling ratio of the hydrogel (S) was calculated by using the equation $S = D/D_0$, where D_0 and D are the diameters of the hydrogel before and after soaking in salt solution, respectively. Small-angle X-ray scattering (SAXS) measurements were carried out on a SAXS point 2.0 (Anton Paar, Austria) apparatus with a wavelength of 0.154 nm and a sample-to-detector distance of 576 mm. The samples with the dimensions of 10 mm (width) × 10 mm (length) × 1 mm (thickness) were sealed with polyimide. One-dimensional scattering intensity curves were gained by azimuthally averaging the two-dimensional scattering patterns. Cryogenic-scanning electron microscopy (cryo-SEM) was performed on a ZEISS Sigma 300 at an accelerating voltage of 3 kV. The hydrogel samples were rapidly frozen in liquid nitrogen for 30 s and then transferred to a preparation chamber in a vacuum (−200 Pa) for spraying a layer of gold onto the cross-section of the samples before measurement. Rheological tests were conducted on a MCR702 rheometer (Anton Paar) with a parallel plate geometry and a fixed gap distance. The samples were cut into discs with a diameter of 8 mm and a height of 2 mm. A constant frequency of 1 Hz and a strain of 0.1% were used for the temperature sweeps. For frequency sweeps, a temperature range of 10–90 °C, a shear strain of 0.1%, and a frequency range of 0.1–100 rad s^{-1} were applied. Based on the principle of time-temperature superposition (TTS), the master curves of energy storage modulus (G') and loss modulus (G'') were built at using 25 °C as the reference temperature. The final frequency range of the master curve depends on the shift factor (a_T) of the hydrogel. The sample edges were sealed with liquid paraffin to prevent water evaporation during measurements. All the tests were repeated three times for three samples in parallel.

2.4 Mechanical testing

Uniaxial tensile experiments were performed using a universal tensile testing machine (Suns MODUTM 4202) with a load cell

of 50 N. Dumbbell-shaped hydrogel samples (thickness = 1 mm, width = 3 mm, length = 15 mm) were tested with a tensile rate of 10 mm min^{-1}. The engineering stress (σ) was defined as the applied force divided by the original cross-sectional area, while the engineering strain (ε) was defined as the length change of the specimen during tension divided by the initial gauge length. The modulus (E) was calculated by taking the slope of the initial linear region of stress–strain curve, and the toughness (Γ) was obtained by integrating the area under the stress–strain curve. The tear energy test was conducted on rectangular samples (thickness = 1.5 mm, width = 50 mm, length = 15 mm) with an initial cut of 20 mm. Both arms of the sample were clamped, and the upper arm was pulled upward at a constant speed of 10 mm min^{-1}. The tear energy (T) was calculated by the equation $T = 2F/w$, where F is the applied force and w is the thickness of the sample. All tests were performed at room temperature in a humid environment and repeated three times.

2.5 Quasi-static puncture tests

ASTM F3007 was employed as a reference for the puncture test setup in this study.[27,28] The puncture tests were conducted using a universal testing machine (Instron 5969 universal machine). Square hydrogel samples (thickness = 0.8 mm, width = length = 40 mm) were fixed between two steel hoops. Then, a loading nose with a spherical tip (stainless steel, diameter = 1 or 4 mm) was slowly penetrated through the center of the samples with a quasi-static velocity of 0.6 mm min^{-1} for the thin tip (diameter = 1 mm), and 0.6 mm min^{-1} and 50 mm min^{-1} for the other tip (diameter = 4 mm) until failure, respectively. The puncture force (F) and puncture displacement (D) were measured during the tests, and the energy to puncture (E_p) was determined by integrating the area under the force–displacement curve. All tests were repeated at least three times.

3. Results and discussion

3.1 Preparation and characterization of hydrogels

The Hofmeister effect based on ions can affect the solubility of polymers, which may be utilized to modulate the aggregation of copolymers in the hydrogel to simply adjust the mechanical properties.[29,30] Due to the strong salting-out effect of sulfate anions,[31,32] we chose Na_2SO_4 as the salt and studied the effect of supersaturated Na_2SO_4 solutions on the pre-prepared hydrogels based on hydrophobic association. The schematic illustration of the preparation process of hydrogels is shown in Fig. 1a. Firstly, P(IMA-*co*-AAm) hydrogel was formed by copolymerizing IMA with AAm in a mixed solvent DMSO/H_2O (10/1, v/v), followed by the solvent exchange of DMSO with water. Then, the hydrogel was immersed in the Na_2SO_4 solutions with different concentrations for two days to produce the P(IMA-*co*-AAm)–Na_2SO_4-*x* hydrogels (*x* is the concentration of Na_2SO_4 solution). The saturated concentration of Na_2SO_4 has been measured to be 2.3 M at room temperature, and it was noted that the supersaturated Na_2SO_4 solutions at room temperature (>2.3 M) were used to investigate the Hofmeister effect of supersaturated solution on the hydrogels. Herein, we prepared the P(IMA_1-*co*-$AAm_{1.5}$)–Na_2SO_4 hydrogel as the typical hydrogel. The ^1H NMR and FTIR spectra of hydrogel show the disappearance of the

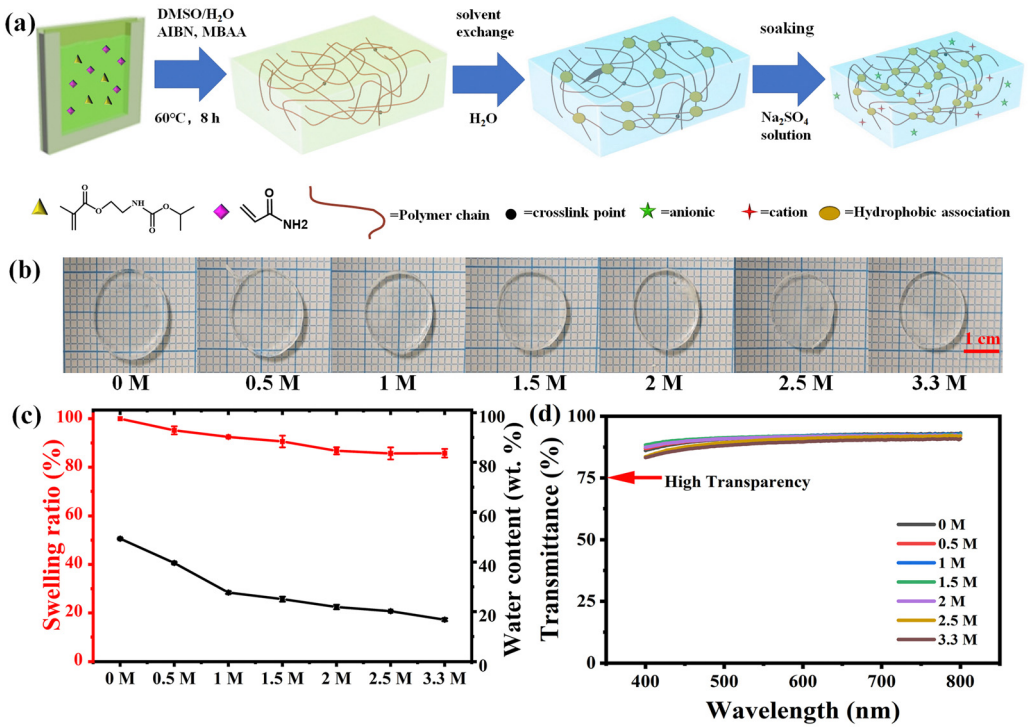

Fig. 1 (a) Schematic illustration for the preparation of P(IMA-*co*-AAm)–Na_2SO_4 hydrogels. (b) Photographs, (c) swelling ratio and water content, and (d) transmittance of P(IMA_1-*co*-$AAm_{1.5}$)–Na_2SO_4 hydrogels prepared in Na_2SO_4 solutions with different concentrations.

proton peaks (5.60 and 6.12 ppm) and vibration peaks (3100 cm^{-1}, 1600 cm^{-1}, and 980 cm^{-1}) of $H_2C{=}C$ bonds and the increase in the proton peak area of $-CH_2-$ (1.7 ppm) (Fig. S1, ESI†), confirming the successful preparation of the hydrogel. Moreover, the FTIR spectra of P(IMA_1-*co*-$AAm_{1.5}$)–Na_2SO_4 hydrogels was similar to that of the pristine hydrogel, indicating that there was no coordination bond between ions and polymers (Fig. S1, ESI†). Compared to the transparent pristine hydrogel, all the P(IMA_1-*co*-$AAm_{1.5}$)–Na_2SO_4 hydrogels were also transparent with a transmittance higher than 80% in the visible range (400–800 nm) and had a small shrinkage lower than 15% with a gradually decreased water content (Fig. 1b–d). As the concentration of Na_2SO_4 solution increased, the transmittance curves of hydrogels almost overlapped with each other, while the swelling ratio of hydrogels showed a small decrease and then became stable when the Na_2SO_4 solutions were supersaturated. These results imply that there is no detectable phase separation in the hydrogel containing Na_2SO_4, but the presence of Na_2SO_4 ions may induce chain contraction in the hydrogels until the Na_2SO_4 solutions are supersaturated. To investigate this, the swelling ratios of the PIMA–Na_2SO_4 hydrogel with only hydrophobic segments and the PAAm–Na_2SO_4 hydrogel with only hydrophilic segments were also measured. With the increasing concentration of Na_2SO_4 solution, there is no shrinkage in the PIMA–Na_2SO_4 hydrogel and its swelling ratio was almost unchanged, while an obvious shrinkage was observed in the PAAm–Na_2SO_4 hydrogel and the shrinkage became stable until the Na_2SO_4 solution was saturated. In comparison, the P(IMA_1–$AAm_{1.5}$)–Na_2SO_4 hydrogels based on hydrophobic and hydrophilic segments showed a small shrinkage. These results indicate that the shrinkage of P(IMA_1-*co*-$AAm_{1.5}$)–Na_2SO_4 was mainly derived from the contraction of hydrophilic segments (Fig. S2, ESI†).

3.2 Microstructure and rheological characterization of hydrogels

To investigate the effect of Na_2SO_4 solution on the microstructures of hydrogels, cryo-SEM and SXAS measurements were carried out on the P(IMA_1-*co*-$AAm_{1.5}$)–Na_2SO_4 hydrogels. As shown in Fig. 2a–g, the homogenous network of hydrogels became more and more compact with the increasing concentration of Na_2SO_4 solution until the salt solution was saturated. The pore surface coverage was statistically calculated using Image J software (Fig. 2h). The porosity of the cross-section surface gradually decreased as the concentration of Na_2SO_4 solution increased and then became stable when the Na_2SO_4 solutions were saturated. These results suggest that the unsaturated Na_2SO_4 solution could gradually increase the cross-linking density of hydrogel with the Na_2SO_4 concentration, while the supersaturated Na_2SO_4 solutions could not further affect the cross-linking density. This tendency was also confirmed by the SAXS results (Fig. 2i), where the peak, ascribed to the distance between hydrophobic associations, gradually shifted to the higher *q*-values when the Na_2SO_4 concentration increased from 0 M to

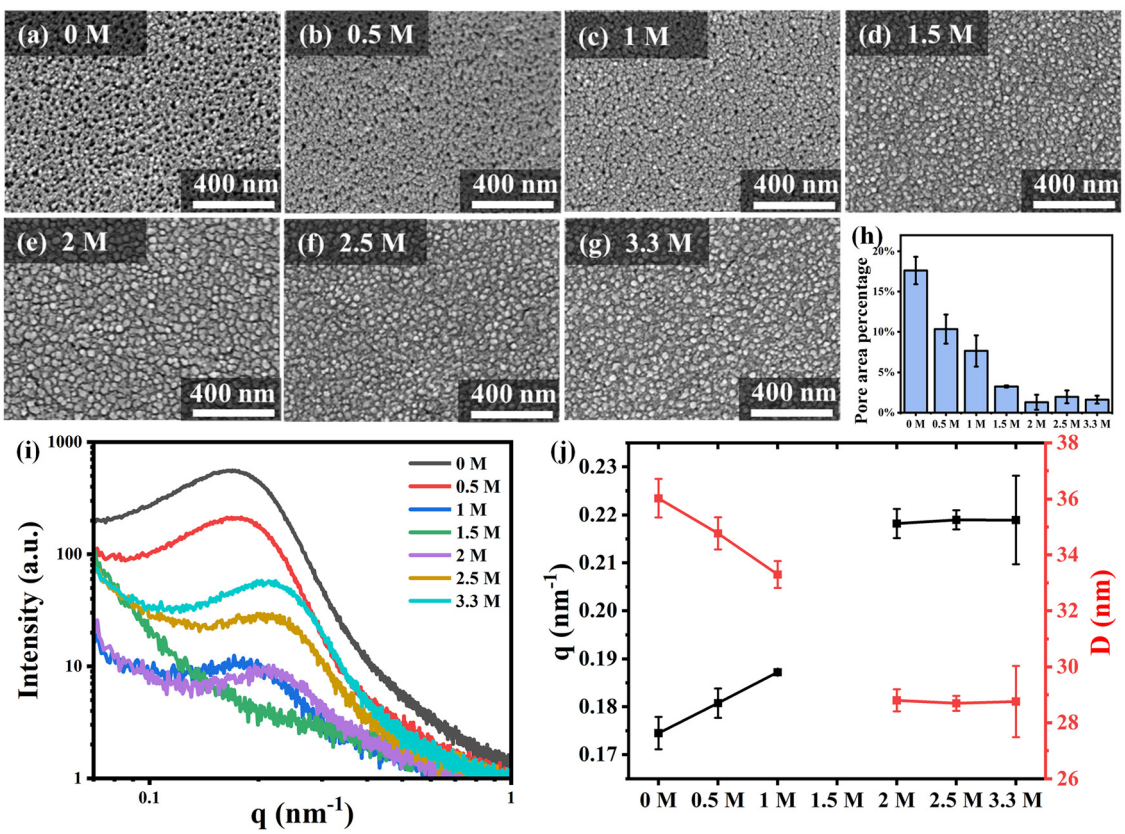

Fig. 2 (a)–(g) Cryo-SEM images, (h) percentage of pore surface area, (i) SAXS profiles, and (j) *q* and *D* of P(IMA_1-*co*-$AAm_{1.5}$)–Na_2SO_4-*x* hydrogels (*x* is 0 M, 0.5 M, 1 M, 1.5 M, 2 M, 2.5 M, and 3.3 M).

1.0 M and then the shift stopped as the Na_2SO_4 solutions were saturated. The calculated average distance (D) between the hydrophobic associations decreased from 36 nm in the P(IMA_1-*co*-$AAm_{1.5}$)–Na_2SO_4-0 hydrogel to 33 nm in the P(IMA_1-*co*-$AAm_{1.5}$)–Na_2SO_4-1 and remained at 29 nm in the hydrogels treated by the supersaturated Na_2SO_4 solutions (Fig. 2j). The change tendency of D with the concentration of Na_2SO_4 solutions was consistent with that of swelling ratio of hydrogels, implying that the increased cross-linking density may be ascribed to the contraction of polymer chains between hydrophobic associations. It was noted that the peak intensity gradually decreased to be undetected as the Na_2SO_4 concentration increased from 0 M to 1.5 M, while it reappeared and increased when the Na_2SO_4 concentration was higher than 2 M. The result implies that the difference of electron cloud density between hydrophobic associations and the surrounding hydrophilic chains was reduced first to become undetected and then increased with the Na_2SO_4 solution thickening, which may be ascribed to the combined effect of the presence of ions and phase separation at different Na_2SO_4 concentrations.[33,34] Taking the small decrease in the D and the obvious change in the peak intensity, we inferred that the dilute ions may be more likely to approach and influence the hydrophilic polymer chains, leading to the decrease in their solubility and the resultant contraction; a high concentration of ions may mainly affect the hydrophobic association, inducing its self-enhancement.

The effect of Na_2SO_4 solution (especially the supersaturated one) on the chain rigidity and viscoelasticity of hydrogels was studied by the rheological measurements. As shown in Fig. 3a, all the hydrogels showed a peak of loss factor (tan δ), corresponding to the glass transition temperature (T_g), which gradually shifted from 33 °C to 53 °C with the concentration of Na_2SO_4 solution increasing. The increase in T_g was ascribed to the salting-out effect of Na_2SO_4 on polymer chains, which improves the interchain interactions and enhances the chain rigidity. It was noted that all the hydrogels are glassy hydrogels at room temperature because their T_g was higher than 33 °C, and the glassy state is beneficial for simultaneously improving the strength, toughness, and modulus of hydrogels.[35,36] This viscoelasticity and glass behaviors were also confirmed by frequency sweep spectra obtained by TTS (Fig. 3b and Fig. S3, ESI†). The temperature dependence of the horizonal shift factor (a_T) showed a non-Arrhenius behavior with two apparent activation energy (E_a) values (Fig. 3c and Fig. S4, ESI†). The higher E_a at the low temperature range corresponded to the mobility of polymer chains between hydrophobic associations, and the lower one at high temperature range reflected the strength of hydrophobic associations. When the concentration of Na_2SO_4 solution increased, the calculated relaxation time and the two E_a were monotonically increased; however, the increase in relaxation time was significant (from 9 s for 0 M to 700 s for 3.3 M) (Fig. S5, ESI†), while the two E_a gave a small increase (Fig. 3d). These results indicated that both the strength of hydrophobic associations and

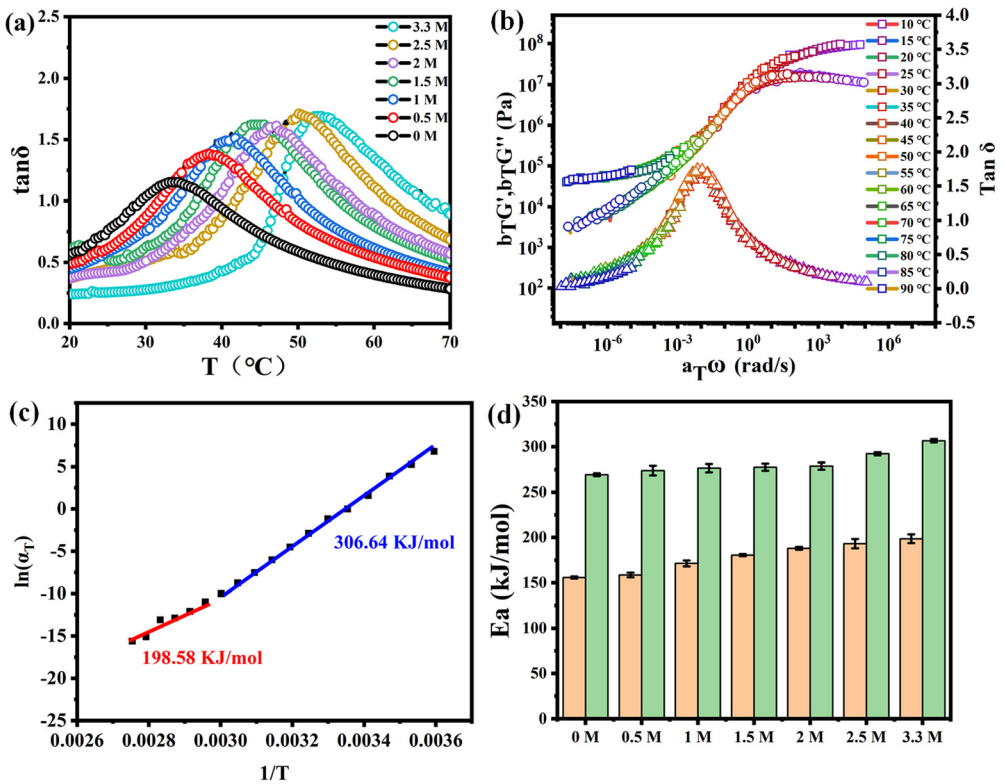

Fig. 3 (a) Tan δ curves of P(IMA_1-*co*-$AAm_{1.5}$)–Na_2SO_4-*x* hydrogels (*x* is 0 M, 0.5 M, 1 M, 1.5 M, 2 M, 2.5 M, and 3.3 M). (b) Spectra of storage modulus (G'), loss modulus (G''), and loss factor (tan δ) and (c) time–temperature shift factors and bi-linearly fitted lines of P(IMA_1-*co*-$AAm_{1.5}$)–Na_2SO_4-3.3M hydrogels. (d) The calculated apparent activation energy (E_a) of different P(IMA_1-*co*-$AAm_{1.5}$)–Na_2SO_4-*x* hydrogels (*x* is 0 M, 0.5 M, 1 M, 1.5 M, 2 M, 2.5 M, and 3.3 M).

the interaction of polymer chains between hydrophobic associations were gradually enhanced by thickening the Na_2SO_4 solution. The obvious increase in the relaxation time of the P(IMA_1-*co*-$AAm_{1.5}$)–Na_2SO_4-3.3 hydrogel was contributed to the double-constraint impact on the network resulting from the strongest hydrophobic associations and interaction of surrounding hydrophilic chains under the supersaturated Na_2SO_4 solution (3.3 M).

Based on the results mentioned above, we can deduce the evolution of the hydrogel network structure with the increase of Na_2SO_4 solution. As shown in Fig. 4, the pristine hydrogel network is composed of the hydrophobic associations and the surrounding hydrophilic chains, where most water molecules are attracted by the hydrophilic chains. Upon immersing in Na_2SO_4 solution, the strong hygroscopicity of the SO_4^{2-} ion could alter the structure and activity of water molecules and cause them to leave the network chains, leading to an increase in the polymer chains interactions ('salting out' effect). Thus, the hydrophilic chains contract and the hydrophobic associations strengthen, bringing about an increase in the cross-linking density and strength. Because hydrophilic chains attract most water molecules, the ions may be more likely to approach the hydrophilic polymer chains, and the salting-out effect is more obvious on hydrophilic polymer chains (big contraction) than that on hydrophobic associations (small enhancement). When the Na_2SO_4 solution is saturated, the contraction of hydrophilic polymer chains stops due to the stability of polymer chains interactions, but the strength of hydrophobic associations is further increased, which may be because more ions could affect the hydrophobic chains. The saturated Na_2SO_4 solution provides a simple and effective method to construct a network with high-density and appropriate-strength hydrophobic associations. This structure would benefit the simultaneous improvement in stiffness, strength, and toughness.

3.3 Mechanical properties of hydrogels

To demonstrate the effect of network structure induced by Na_2SO_4 solution on the mechanical performance of the hydrogels, uniaxial tensile tests were carried out on the P(IMA-*co*-AAm)–Na_2SO_4 hydrogels with different monomer ratios and concentrations of Na_2SO_4 solution. The immersing time was fixed at 48 h because the mechanical properties of hydrogels were stable after 48 h soaking in Na_2SO_4 solution (Fig. S6, ESI†). The stress–strain curves of the P(IMA_1-*co*-$AAm_{1.5}$)–Na_2SO_4-*x* hydrogels are shown in Fig. 5a. Compared to the soft and weak pristine hydrogel, the hydrogels after immersing Na_2SO_4 solution showed an obvious yielding phenomenon, and the yielding strength was significantly enhanced from 0 MPa (0 M) to 17 MPa (3.3 M). It suggests that the P(IMA_1-*co*-$AAm_{1.5}$)–Na_2SO_4 hydrogels were in the glassy state at room temperature and became stronger and stiffer with the increase in Na_2SO_4 solution, which was consistent with the results of tan δ. More importantly, the modulus (E), fracture strength (σ), and toughness (Γ) simultaneously and greatly increased in the single hydrogel with the concentrations of Na_2SO_4 solution. As shown in Fig. 5b and c, P(IMA_1-*co*-$AAm_{1.5}$)–Na_2SO_4-3.3 hydrogel had a remarkable E of 253 ± 7 MPa, a σ of 12.65 ± 0.07 MPa, and a Γ of 19.6 ± 3.2 MJ m^{-3}, in which E, σ, and Γ were 25, 4, and 4 times higher than that of pristine one (E = 8.6 ± 2.4 MPa, σ = 2.73 ± 0.42 MPa, and Γ = 4.6 ± 1.2 MJ m^{-3}). The similar increase tendency of the mechanical properties with the concentration of Na_2SO_4 solution was also observed in the P(IMA-*co*-AAm)–Na_2SO_4-*x* hydrogels with different molar ratios, hydrogels with other hydrophobic monomers (P(BA_1-AAm_1)–Na_2SO_4-*x* and P($2EA_1$-AAm_1)–Na_2SO_4-*x* hydrogels), and hydrophilic PAAm–Na_2SO_4-*x* hydrogels (Fig. S7 and S8, ESI†). However, the improvement of mechanical performance was limited in the PAAm–Na_2SO_4 hydrogel, and it was still weak because of the weak interaction between PAAm chains. These results indicate that the increase in mechanics of P(IMA_1-*co*-$AAm_{1.5}$)–Na_2SO_4 was attributed to the high-density and strong hydrophobic associations induced by Na_2SO_4, which not only withstand the applied load at the initial deformation due to the rigid chains and strong cross-links, but also bear heavy load and dissipate much more energy at large deformation owing to the adaptive destruction of strong dynamic cross-links.

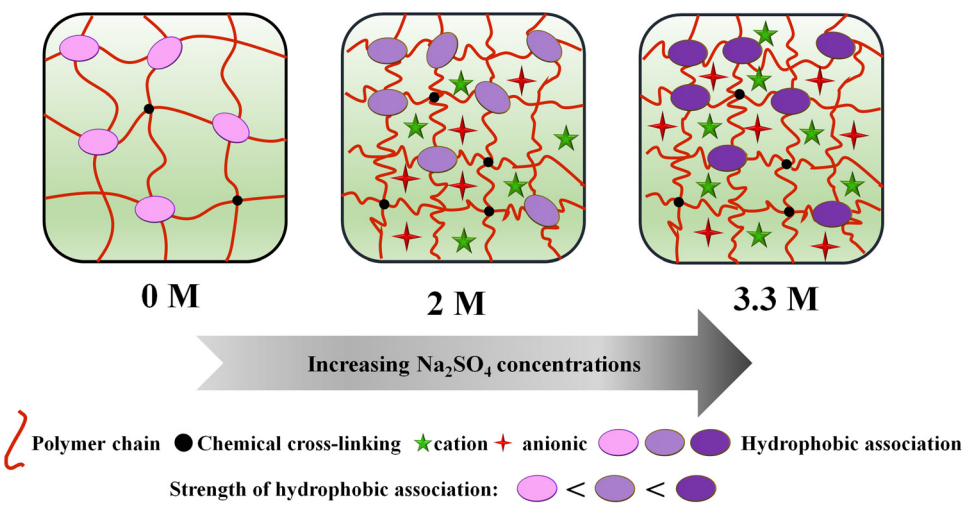

Fig. 4 Schematic illustration of hydrophobic associations and the surrounding hydrophilic chains in the P(IMA_1-*co*-$AAm_{1.5}$)–Na_2SO_4 hydrogels.

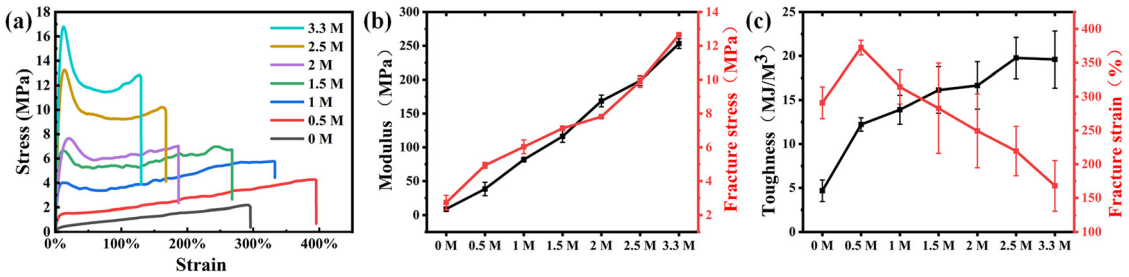

Fig. 5 (a) Tensile stress–strain curves, (b) Young's modulus and fracture stress, and (c) toughness and fracture strain of P(IMA$_1$-*co*-AAm$_{1.5}$)–Na$_2$SO$_4$-*x* hydrogels (*x* is 0 M, 0.5 M, 1 M, 1.5 M, 2 M, 2.5 M, and 3.3 M).

Thus, the network with high-density and appropriate-strength hydrophobic associations can balance the contradictory needs of different mechanical properties for the structure and greatly improve the mechanical performance, especially the simultaneously enhancement in the stiffness, strength, and toughness.

3.4 Puncture and tear resistance of hydrogels

The practical application of hydrogel materials requires good resistance to mechanical damage, which can expand their application range and extend their service life. To test the capability of P(IMA$_1$-*co*-AAm$_{1.5}$)–Na$_2$SO$_4$ hydrogels to resist mechanical damage, we tested the puncture resistance and tear resistance of the hydrogels. As shown in Fig. 6a, the maximum puncture force (F_{max}) significantly increased from 16 N for the pristine hydrogel to 66 N for the one treated by the supersaturated Na$_2$SO$_4$ solution (3.3 M). The puncture displacement decreased with the increase in concentration of Na$_2$SO$_4$ solution, and the resultant puncture energy (E_p) increased first and then decreased with the highest value of 420 mJ in P(IMA$_1$-*co*-AAm$_{1.5}$)–Na$_2$SO$_4$-1.5 (Fig. 6b). It was noted that the puncture energy and force of our hydrogels were obviously higher than that of many strong hydrogels (Fig. 6c). The puncture resistance was further examined at higher speed and by using a thinner needle (Fig. S9 and S10, ESI†). As the Na$_2$SO$_4$ concentration increased, the F_{max} and E_p gained at 50 mm min^{-1} showed a similar tendency to that got at 0.6 mm min^{-1}. The hydrogel tested at 50 mm min^{-1} was a little stiffer with the highest F_{max} of 75 N and a lower E_p of 240 mJ in the P(IMA$_1$-*co*-AAm$_{1.5}$)–Na$_2$SO$_4$-3.3. Meanwhile, the hydrogels also displayed obvious puncture resistance against the needle with a diameter of 1 mm, where P(IMA$_1$-*co*-AAm$_{1.5}$)–Na$_2$SO$_4$-3.3 remained intact (Fig. 6d). The hydrogels immersing in the Na$_2$SO$_4$ solution also showed enhanced tearing resistance (Fig. 6e and f). The tearing energy gradually increased to 34 kJ m^{-2} with the increase in Na$_2$SO$_4$ concentration, and a piece of P(IMA$_1$-*co*-AAm$_{1.5}$)–Na$_2$SO$_4$-3.3 with a hole can sustain a weight of 2.5 kg without

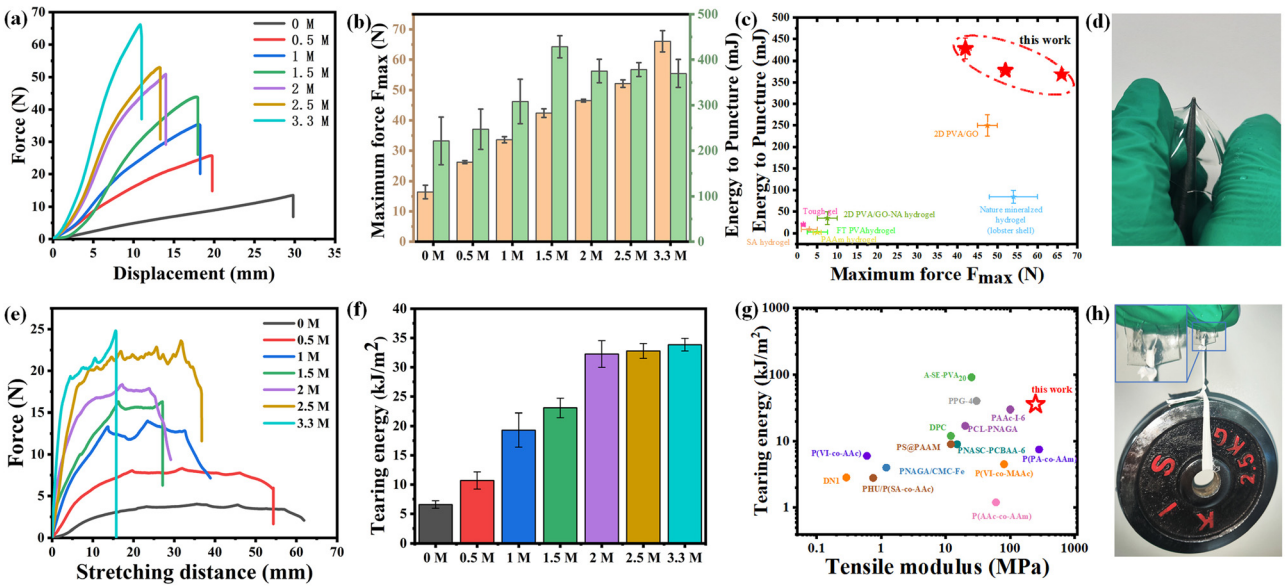

Fig. 6 (a) Puncture force–displacement curves, and (b) the maximum puncture force (F_{max}) and energy to puncture (E) for P(IMA$_1$-*co*-AAm$_{1.5}$)–Na$_2$SO$_4$-*x* hydrogels. (*x* is 0 M, 0.5 M, 1 M, 1.5 M, 2 M, 2.5 M, and 3.3 M). (c) Property maps of the energy to puncture *versus* maximum force (F_{max}) for various hydrogel materials.[27,37] (d) Optical images of the P(IMA$_1$-*co*-AAm$_{1.5}$)–Na$_2$SO$_4$-3.3 hydrogel (30 mm × 15 mm × 1 mm) being punctured by a needle (diameter = 1 mm). (e) The force–displacement curves, and (f) corresponding tearing energy of for P(IMA$_1$-*co*-AAm$_{1.5}$)–Na$_2$SO$_4$-*x* hydrogels (*x* is 0 M, 0.5 M, 1 M, 1.5 M, 2 M, 2.5 M, and 3.3 M). (g) Property maps of the tearing energy *versus* tensile modulus for various hydrogel materials.[10,38–49] (h) Optical images of the P(IMA$_1$-*co*-AAm$_{1.5}$)–Na$_2$SO$_4$-3.3 hydrogel (30 mm × 15 mm × 1 mm) sustaining a weight of 2.5 kg.

crack propagation (Fig. 6h). The improvement tendency of tearing energy is consistent with that of crosslinking density, implying that the high-density physical crosslinking limited the expansion of cracks in the tearing process. The hydrogel treated by the supersaturated Na_2SO_4 solution (3.3 M) displayed comparable modulus and tearing energy with that of many anti-tearing hydrogels (Fig. 6g). These results indicate that the network of high-density and strong hydrophobicity associations endow hydrogels with excellent mechanical properties, which in turn give hydrogel materials good puncture and tear resistance.

4. Conclusions

In conclusion, we constructed an ultra-stiff, strong, and tough hydrogel based on high-density and suitably strong hydrophobic associations by utilizing the Hofmeister effect of supersaturated salt solution on the aggregation of copolymers. The hydrogels were prepared by immersing the pre-formed P(IMA-AAm) hydrogels in Na_2SO_4 solutions. The increase in Na_2SO_4 concentration enhanced the copolymer chain interaction, leading to the contraction of hydrophilic chains until the Na_2SO_4 was saturated and the improvement of hydrophobic associations up to supersaturated Na_2SO_4. Both changes in the copolymer chains brought about an increase in the density and strength of hydrophobic associations in the network, which simultaneously improved the stiffness, strength, and toughness of hydrogels. Due to the high-density and appropriate strength of hydrophobic associations, the P(IMA_1-*co*-$AAm_{1.5}$)–Na_2SO_4-3.3 hydrogel was transparent and showed an E value of 253 ± 7 MPa, a σ of 12.65 ± 0.07 MPa, and a Γ of 19.6 ± 3.2 MJ m^{-3}. It also displayed remarkable puncture and tear resistance with a puncture force of 66 N, a puncture energy of 370 mJ, and a tearing energy of 34 kJ m^{-2}. This work offers a straightforward approach to simultaneously enhance the contradictory mechanical properties of hydrogels, endowing hydrogels with remarkable puncture and tear resistance, which would benefit their applications as puncture-resistant and load-bearing materials.

Data availability

The data supporting this article have been included as part of the ESI.†

Conflicts of interest

There are no conflicts to declare.

References

1 X. Li and J. P. Gong, *Nat. Rev. Mater.*, 2024, **9**, 380–398.
2 X. Zhao, X. Chen, H. Yuk, S. Lin, X. Liu and G. Parada, *Chem. Rev.*, 2021, **121**, 4309–4372.
3 S. Zhao, Y. Zuo, T. Liu, S. Zhai, Y. Dai, Z. Guo, Y. Wang, Q. He, L. Xia, C. Zhi, J. Bae, K. Wang and M. Ni, *Adv. Energy Mater.*, 2021, **11**, 2101749.
4 X. Zhao, M. Wang, Y. Chen, Z. Chen, T. Suo, W. Qian, J. Hu, X. Song, W.-N. Mei, R. Sabirianov and L. Tan, *ACS Appl. Mater. Interfaces*, 2019, **11**, 19421–19428.
5 X. Kuang, M. O. Arıcan, T. Zhou, X. Zhao and Y. S. Zhang, *Acc. Mater. Res.*, 2022, **4**, 101–114.
6 X. Dai, Y. Zhang, L. Gao, T. Bai, W. Wang, Y. Cui and W. Liu, *Adv. Mater.*, 2015, **27**, 3566–3571.
7 Z. Han, P. Wang, Y. Lu, Z. Jia, S. Qu and W. Yang, *Sci. Adv.*, 2022, **8**, 5066.
8 H. C. Yu, S. Y. Zheng, L. Fang, Z. Ying, M. Du, J. Wang, K. F. Ren, Z. L. Wu and Q. Zheng, *Adv. Mater.*, 2020, **32**, 2005171.
9 T. L. Sun, T. Kurokawa, S. Kuroda, A. B. Ihsan, T. Akasaki, K. Sato, M. A. Haque, T. Nakajima and J. P. Gong, *Nat. Mater.*, 2013, **12**, 932–937.
10 M. T. I. Mredha, S. K. Pathak, V. T. Tran, J. Cui and I. Jeon, *Chem. Eng. J.*, 2019, **362**, 325–338.
11 L. Yang, S. Li, Z. Zhao, J. Wang, H. Lv and X. Yang, *Polym. Chem.*, 2023, **14**, 2212–2219.
12 D. C. Tuncaboylu, M. Sari, W. Oppermann and O. Okay, *Macromolecules*, 2011, **44**, 4997–5005.
13 F. Wang and R. A. Weiss, *Macromolecules*, 2018, **51**, 7386–7395.
14 N. Rauner, M. Meuris, M. Zoric and J. C. Tiller, *Nature*, 2017, **543**, 407–410.
15 M. Milovanovic, N. Isselbaecher, V. Brandt and J. C. Tiller, *Chem. Mater.*, 2021, **33**, 8312–8322.
16 L. Xu, Y. Qiao and D. Qiu, *Adv. Mater.*, 2023, **35**, 2209913.
17 X. N. Zhang, C. Du, Y. J. Wang, L. X. Hou, M. Du, Q. Zheng and Z. L. Wu, *Macromolecules*, 2022, **55**, 7512–7525.
18 Y. Huang, L. Xiao, J. Zhou, T. Liu, Y. Yan, S. Long and X. Li, *Adv. Funct. Mater.*, 2021, **31**, 2103917.
19 S. Tan, C. Wang, B. Yang, J. Luo and Y. Wu, *Adv. Mater.*, 2022, **34**, 2206904.
20 T. Li, X. Li, J. Yang, H. Sun and J. Sun, *Adv. Mater.*, 2023, **35**, 2307990.
21 V. T. Tran, M. T. I. Mredha and I. Jeon, *Extreme Mech. Lett.*, 2020, **37**, 100691.
22 X. Lin, X. Wang, H. Cui, G. Ouyang and H. Guo, *Chem. Eng. J.*, 2023, **457**, 141280.
23 H. Guo, T. Nakajima, D. Hourdet, A. Marcellan, C. Creton, W. Hong, T. Kurokawa and J. P. Gong, *Adv. Mater.*, 2019, **31**, 1900702.
24 X. Yang, H. Cui, Z. Wang, W. Wang, H. Guo and X. Wang, *Polym. Test.*, 2023, **124**, 108103.
25 X. Yu, Z. Qin, H. Wu, H. Lv and X. Yang, *Macromolecules*, 2019, **52**, 1249–1256.
26 L. X. Hou, H. Ju, X. P. Hao, H. Zhang, L. Zhang, Z. He, J. Wang, Q. Zheng and Z. L. Wu, *Adv. Mater.*, 2023, **35**, 2300244.
27 X. Liang, G. Chen, I. M. Lei, P. Zhang, Z. Wang, X. Chen, M. Lu, J. Zhang, Z. Wang, T. Sun, Y. Lan and J. Liu, *Adv. Mater.*, 2022, **35**, 2207587.
28 Z. Yin, F. Hannard and F. Barthelat, *Science*, 2019, **364**, 1260–1263.
29 M. Jaspers, A. E. Rowan and P. H. J. Kouwer, *Adv. Funct. Mater.*, 2015, **25**, 6503–6510.

30 Y. Jin, S. Lu, X. Chen, Q. Fang, X. Guan, L. Qin, C. Chen and C. Zhao, *Macromolecules*, 2024, **57**, 2746–2755.
31 Y. Zhang and P. Cremer, *Curr. Opin. Chem. Biol.*, 2006, **10**, 658–663.
32 Y. Zhang, S. Furyk, D. E. Bergbreiter and P. S. Cremer, *J. Am. Chem. Soc.*, 2005, **127**, 14505–14510.
33 A. Guinier and G. r Fournet, *Small-angle scattering of X-rays*, Wiley, New York, 1955.
34 O. Glatter and O. Kratky, *Small Angle X-ray Scattering*, Academic, London, 1982.
35 J. Hu, C. Du, X. Zhang, Q. Zheng and Z. Wu, *Acta Polym. Sin.*, 2023, **54**, 1795–1816.
36 Y. J. Wang, X. N. Zhang, Y. Song, Y. Zhao, L. Chen, F. Su, L. Li, Z. L. Wu and Q. Zheng, *Chem. Mater.*, 2019, **31**, 1430–1440.
37 J.-Y. Sun, X. Zhao, W. R. K. Illeperuma, O. Chaudhuri, K. H. Oh, D. J. Mooney, J. J. Vlassak and Z. Suo, *Nature*, 2012, **489**, 133–136.
38 W. Li, S. Zheng, X. Zou, Y. Ren, Z. Liu, W. Peng, X. Wang, D. Liu, Z. Shen, Y. Hu, J. Guo, Z. Sun and F. Yan, *Adv. Funct. Mater.*, 2022, **32**, 2207348.
39 Q. Zhang, Z. Xu, X. Zhang, C. Liu, R. Yang, Y. Sun, Y. Zhang and W. Liu, *Adv. Funct. Mater.*, 2022, **32**, 2200360.
40 N. Tang, Y. Jiang, K. Wei, Z. Zheng, H. Zhang and J. Hu, *Adv. Mater.*, 2023, **36**, 2309576.
41 C. Fan, Z. Xu, T. Wu, C. Cui, Y. Liu, B. Liu, J. Yang and W. Liu, *Biomater. Sci.*, 2021, **9**, 5116–5126.
42 P. Jiang, P. Lin, C. Yang, H. Qin, X. Wang and F. Zhou, *Chem. Mater.*, 2020, **32**, 9983–9995.
43 Y. Tian, C. Du, B. Liu, H. N. Qiu, X. H. Zhang, Z. L. Wu and Q. Zheng, *J. Polym. Sci.*, 2021, **59**, 904–911.
44 X. N. Zhang, Y. J. Wang, S. Sun, L. Hou, P. Wu, Z. L. Wu and Q. Zheng, *Macromolecules*, 2018, **51**, 8136–8146.
45 F. Zhu, S. Feng, Z. Wang, Z. Zuo, S. Zhu, W. Yu, Y. N. Ye, M. An, J. Qian, Z. L. Wu and Q. Zheng, *Macromolecules*, 2023, **56**, 5881–5890.
46 H. Ding, X. N. Zhang, S. Y. Zheng, Y. Song, Z. L. Wu and Q. Zheng, *Polymer*, 2017, **131**, 95–103.
47 H. Li, H. Wang, D. Zhang, Z. Xu and W. Liu, *Polymer*, 2018, **153**, 193–200.
48 Z. Wang, X. Zheng, T. Ouchi, T. B. Kouznetsova, H. K. Beech, S. Av-Ron, T. Matsuda4, B. H. Bowser, S. Wang, J. A. Johnson, J. A. Kalow, B. D. Olsen, J. Gong, M. Rubinstein and S. L. Craig, *Science*, 2021, **374**, 193–196.
49 S. Y. Zheng, Y. Tian, X. N. Zhang, M. Du, Y. Song, Z. L. Wu and Q. Zheng, *Soft Matter*, 2018, **14**, 5888–5897.